Renewable and Sustainable Energy Reviews 34 (2014) 194–207

Contents lists available at ScienceDirect

Renewable and Sustainable Energy Reviews

journal homepage: www.elsevier.com/locate/rser

Improving grid integration of wind turbines by using secondary batteries

Raúl Sarrias-Mena [a], Luis M. Fernández-Ramírez [a,*], Carlos A. García-Vázquez [a], Francisco Jurado [b]

[a] Research Group in Electrical Technologies for Sustainable and Renewable Energy (PAIDI-TEP-023), Department of Electrical Engineering, EPS Algeciras, University of Cadiz, Avda. Ramón Puyol, s/n, 11202 Algeciras, Cádiz, Spain

[b] Research Group in Research and Electrical Technology (PAIDI-TEP-152), Department of Electrical Engineering, EPS Linares, University of Jaen, C/Alfonso X, No 28, 23700 Linares, Jaén, Spain

ARTICLE INFO

Article history:
Received 28 November 2011
Received in revised form
24 January 2014
Accepted 1 March 2014
Available online 27 March 2014

Keywords:
DFIG wind turbine
Battery
Wind power
Grid integration

ABSTRACT

Energy storage systems (ESSs) appear as a viable solution to some of the stability and intermittency problems of wind power generation. As a consequence, it is crucial to develop adequate control strategies that allow the coordinate operation of both energy sources. Moreover, in order to minimize the impact of large wind farms on the power system, many countries have set strict grid codes that wind power generators must accomplish. Hence, it is also necessary to pay due attention to the fault ride through capabilities of these hybrid systems. In this paper two different hybrid configurations are modeled in MATLAB/Simulink, consisting on a doubly fed induction generator driven wind turbine and electrochemical batteries as ESS. They are simulated and compared under various operating conditions (i.e. real fluctuating wind speed input with variable active and reactive power grid demand, voltage sags, three-phase and single-phase fault to ground, and overvoltage). A conventional wind turbine without ESS is also considered as a base-case in order to highlight the main benefits of the hybrid schemes. The results show that by implementing one of the presented control strategies, it is possible to enhance the response to faults of the hybrid systems, achieving higher active power injection and helping the recovery to steady-state, thus improving the grid connection capabilities of hybrid wind farms.

Contents

* Corresponding author. Tel.: +34 956 028166; fax: +34 956 028014.
E-mail addresses: raul.sarrias@uca.es (R. Sarrias-Mena), luis.fernandez@uca.es (L.M. Fernández-Ramírez), carlosandres.garcia@uca.es (C.A. García-Vázquez), fjurado@ujaen.es (F. Jurado).

http://dx.doi.org/10.1016/j.rser.2014.03.001
1364-0321/

1. Introduction

Currently, renewable energies are experiencing a considerable growth in an attempt to reduce the energetic dependency on fossil fuels, and subsequent greenhouse emissions, that the vast majority of the industrialized countries have to cope with nowadays [1,2]. Among many different alternatives, wind power stands out as a reliable and frequent election in both developed and developing regions [1–4]. Therefore, intensive research is currently being done in the field of economic, social, environmental and political aspects of renewable resources, many focusing particularly on wind energy [5–8]. Nevertheless, increasing penetration of wind power generation poses a challenge for the proper operation of the electricity network [9,10], due to the inherent intermittency and lack of control of this natural resource.

The use of energy storage systems (ESSs) coupled to wind power can enhance the grid-connection capability of this supply [9–11]. Nowadays, there are various storage technologies available. All of them present particular characteristics and show a different performance. Hence, it is not possible to clearly identify any of them as the best option among the others, since their adequacy depends on the specific requirements of every application. According to [12,13], by the end of the year 2010 the pumped hydro storage (PHS) recorded 99% of the worldwide electric energy storage capacity with 127 GW, followed by compressed air energy storage (CAES) with 440 MW. Batteries such as sodium-sulfur (NaS) and lead-acid, ranked, respectively, third and fourth with 316 MW and 35 MW. Other technologies, such as flywheels, as well as nickel-cadmium, lithium-ion and redox-flow batteries achieved lower registers in this study. Regarding PHS and CAES, these systems need special infrastructure for the large water and air reservoirs. Thus, their use may be restricted to suitable locations of the wind farm. On the other hand, installation of batteries is more flexible and adaptable. They can even be integrated within the wind turbine operating system [14], as in the hybrid configuration considered in this study. For these reasons, the use of PHS or CAES as storage system was declined in this paper. Amongst batteries, NaS and lead-acid are both well-developed technologies. Research on the latter has been carried out for over 140 years [15], thus being the most mature battery type [16–18]. Notwithstanding, their features are still improving nowadays, and advanced lead-acid batteries are a promising alternative in the near future [12,19,20]. Considering the costs derived from energy storage, they are highly dependable on the rated power, capacity, and projected application of the device [12,13]. Furthermore, in many technologies they are expected to vary substantially in the forthcoming future. Nonetheless, for similar characteristics, today lead-acid is a cost-competitive technology among other types of batteries [15,21,22]. Also, the implementation of lead-acid batteries coupled to wind farms and other renewable resources has been recorded in several real-scale projects [23], which validate the operational capability of this technology for such applications. Regarding the relevant qualities of lead-acid batteries stated here, these storage devices have been chosen for the hybrid system considered in this paper.

Currently, wind turbines based on doubly fed induction generator (DFIG) are broadly used in large variable-speed wind farms, as well as in standalone applications [24–26]. Their configuration with a partial-scale power converter (instead of a full-scale), which reduces costs and losses in the generator, is one of the main advantages of this technology [24,27]. The ability to perform a decoupled control of active and reactive power generation is also a remarkable characteristic of DFIGs. This feature can be easily achieved by implementing vector control on the DFIG power converters [27,28]. This type of generator has a large capacity to absorb or provide reactive power [29–31]. Therefore, the control systems implemented on the power converters should grant an adequate adaptability to varying grid requirements, and offer grid support through reactive power management in both steady-state operation and during faults. This becomes more necessary since the grid codes in many countries require the wind farms to remain connected even under severe low voltage conditions [32,33].

Storage devices in hybrid systems play also an important role in this respect. Due to their availability to exchange active power, they are able to perform power management according to grid requirements, but they can also contribute to the fault ride-through (FRT) capabilities of wind turbines. So far, very few studies have dealt with the dynamic behavior of these hybrid systems under both situations. Jiang et al. [34] developed a dynamic model of a DFIG with ESS. A battery connected to the DC bus of the DFIG compensated the power imbalance between the inputted mechanical power to the wind turbine, and the references set for the rotor side converter (RSC) and grid side converter (GSC) of the generator. Nonetheless, the hybrid system in [34] lacked of a supervisory control system to coordinate the operation of the ESS and the DFIG, thus not taking into account the state-of-charge (SOC) of the battery. Moreover, the response of the hybrid system to grid faults was not presented. A similar concept with different implementation was addressed in [35,36], where the battery was directly attached to the DC bus of the DFIG without a DC/DC converter. This configuration poses two major concerns: (i) higher voltage requirements for the battery and (ii) there are less controllable parameters in the coordinated control strategy. Hence, a scheme with DC/DC converter was preferred in this paper. In [37], supercapacitors (SCs) were used instead of batteries. An adequate performance of the hybrid DFIG-SC system was achieved for active power smoothing and grid demand commitment. However, reactive power management or FRT capabilities of the system under study were not addressed. Variations to these schemes can be found in [38,39]. In [38], a dummy load was included in a remote area supply hybrid system in order to absorb over-generation that could not be stored in the battery. Yang et al. [39] proposed a battery ESS divided in two blocks which were controlled for different purposes. Nevertheless, none of these studies evaluated the dynamic performance of the hybrid systems under faulty network conditions. Other authors [40–42] focused on the FRT enhancement of hybrid wind/ESS systems, but did not evaluate their control strategies for tracking variable active/reactive power grid demand. In [40], a battery absorbed the excess power in the DC bus of a DFIG wind turbine in a voltage sag. This strategy avoided dangerous increase of the DC voltage, but it did not support the power system. Since the ESS was not compelled to provide extra power injection during the fault, a damping effect of the active power drop in the grid could not be

achieved. A different concept was proposed in [41], where a SC was connected to the DFIG output terminals through a STATCOM. This configuration allows the decoupled control of active and reactive power through the proper operation of both devices. This solution augments the FRT capabilities of the wind turbine, although economic aspects should be considered in practical implementation due to the need for several power converters. External location of a small-sized energy capacitor system in a DFIG was also proposed in [42]. With this ESS, the power oscillations and transient behavior during and after a grid fault were improved in the system under analysis. Nevertheless, simulations during no-fault conditions were not shown. Not many studies deal with both the FRT and dynamic grid commitment performance under fluctuating wind speed. In [43,44], DFIG wind turbines equipped with SCs were simulated under variable wind speed and also submitted to grid disturbances. Nonetheless, the ESSs were employed for output power smoothing duties, and the grid requirements were not considered as inputs in the proposed control systems, since batteries are a more adequate alternative for such long-term power supply.

The main aim and novelty of this paper is to show a complete comparative analysis of two different control schemes for hybrid wind/battery systems. In both configurations, a battery ESS is connected through a bidirectional DC/DC converter to the DC bus of the power converter of a 1.5 MW DFIG wind turbine. The DFIG wind turbine without ESS has been considered as a base-case to contrast the improvements accomplished in the hybrid schemes. The systems are required to respond to variations in the grid demand, thus operating similarly to conventional power plants. The study includes the control of active and reactive power generation according to grid demand under real fluctuating wind speed, exploiting the stator and GSC reactive power exchange capacity, and using the ESS to adapt to the active power grid requirements. The supervisory control system implemented allows coordinated operation of the wind turbine and ESS, while overseeing the battery SOC between recommended values. The analysis evaluates the response of hybrid systems to normal operation under fluctuating wind speed and different grid faults (voltage sag, three-phase fault to ground, single-phase fault to ground, and overvoltage). Therefore, a wide range of possible operating conditions are analyzed and compared in order to establish the most suitable control scheme for hybrid wind turbine/battery systems.

The configurations of the wind turbines considered in this work are presented in Section 2. In Section 3, the modeling of the DFIG wind turbine is described, whereas the modeling of the ESS is explained in Section 4. Section 5 presents in detail the control strategies analyzed in this work. The supervisory control system that manages the overall operation of the hybrid systems is explained in Section 6. The simulations results and discussion are illustrated in Section 7. Finally, Section 8 gives the conclusions derived from this work.

2. DFIG wind turbine and ESS

DFIG wind turbine uses a wound rotor induction generator coupled to the wind turbine rotor through a gearbox. The wind turbine includes blade pitch angle control in order to limit the power extracted from the wind.

The induction generator presents the stator winding coupled directly to the grid and a bidirectional power converter feeding the rotor winding. This power converter decouples the electrical grid frequency and the mechanical rotor frequency, enabling the variable speed generation [26,45,46]. The power converter is made up of two back-to-back IGBT bridges linked by a DC bus. The RSC converts the variable frequency of the AC rotor currents into DC currents at the DC bus. The GSC allows the active and reactive power flow to/from the grid, and therefore, its output must adapt to grid voltage and frequency requirements. A DC link capacitor is placed in the DC bus to stabilize voltage. In addition, a crowbar protection is included to avoid excessively high rotor currents flow through the RSC during grid faults. Fig. 1a shows the DFIG wind turbine configuration.

With the configuration described, the wind turbine is not capable of regulating the active power generation independently from incoming wind speed. Nonetheless, it can be achieved by integrating an ESS in the wind turbine. This paper proposes the use of an electrochemical battery connected to the DC bus of the DFIG through a bidirectional DC/DC converter, as shown in Fig. 1b. The battery exchanges energy with the DC bus, enabling its charge or discharge. When the battery is being charged, it stores energy sourced from the RSC. This stored energy can be released to the grid through the GSC, supplementing the wind turbine generation. The DC link capacitor is charged/discharged by the RSC, GSC and battery currents.

3. Modeling of the DFIG wind turbine

A General Electric (GE) 1.5 MW DFIG wind turbine [47] was considered in this work. The model of this wind turbine, which will be described next, is composed of the following subsystems: (1) mechanical system and (2) electrical system. The model is based on the wind turbine model included in SimPowerSystems® of MATLAB [48]. Modifications on that model have been performed to apply the different control strategies presented in this paper, as well as to simulate the combined operation of the wind turbine and the battery.

3.1. Mechanical system model

The mechanical system consists of the aerodynamic rotor and drive train. The rotor model expresses the mechanical torque extracted from the wind, defined by the actuator disk theory [49]. This torque is transmitted to the DFIG rotor through the drive train, represented by the well-known two masses model [49]. In this model, two rotating masses –the aerodynamic rotor and the DFIG rotor– are elastically connected via springs, characterized by the stiffness and damping factor of the coupling.

3.2. Electrical system model

Two main components can be identified in the electrical system model: the DFIG and its power converter.

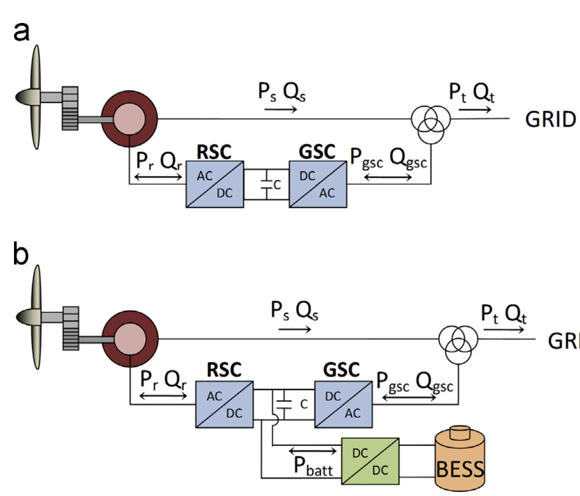


Fig. 1. (a) DFIG wind turbine and (b) DFIG wind turbine with ESS based on battery.

3.2.1. DFIG

The behavior of the DFIG is defined by a fifth-order model [50]. It consists of four electrical differential equations (two equations for each the stator and rotor voltage) expressed in a direct (d)-quadrature (q) coordinate reference frame rotating at synchronous speed ω_s, and one mechanical differential equation, included in the drive train model. According to this model, the stator and rotor voltage d-q components can be expressed as follows:

$$\begin{aligned} u_{ds} &= R_s \cdot i_{ds} + \frac{d}{dt}\varphi_{ds} - \omega \cdot \varphi_{qs} \\ u_{qs} &= R_s \cdot i_{qs} + \frac{d}{dt}\varphi_{qs} + \omega \cdot \varphi_{ds} \end{aligned} \quad (1)$$

$$\begin{aligned} u_{dr} &= R_r \cdot i_{dr} + \frac{d}{dt}\varphi_{dr} - (\omega - \omega_r) \cdot \varphi_{qr} \\ u_{qr} &= R_r \cdot i_{qr} + \frac{d}{dt}\varphi_{qr} + (\omega - \omega_r) \cdot \varphi_{dr} \end{aligned} \quad (2)$$

where u denotes voltage, i denotes current, ω is rotating speed, φ represents magnetic flux, R denotes resistance and L inductance, indexes d and q stand for the direct and quadrature components, and indexes s and r refer to stator and rotor, respectively.

Furthermore, the stator and rotor magnetic flux linkages are given by

$$\begin{aligned} \varphi_{ds} &= L_s \cdot i_{ds} + L_m \cdot i_{dr} \\ \varphi_{qs} &= L_s \cdot i_{qs} + L_m \cdot i_{qr} \end{aligned} \quad (3)$$

$$\begin{aligned} \varphi_{dr} &= L_r \cdot i_{dr} + L_m \cdot i_{ds} \\ \varphi_{qr} &= L_r \cdot i_{qr} + L_m \cdot i_{qs} \end{aligned} \quad (4)$$

where index m stands for magnetizing. All the magnitudes in Eqs. (1)–(4) are used in the *per unit* (pu) system in the implemented model.

3.2.2. Power converter

The power converter used in the DFIG wind turbine is made up of two back-to-back IGBT bridges linked by a DC bus, where the DC voltage is stabilized by a link capacitor. The converter is modeled as an AC/DC/AC PWM converter based on IGBT switches.

Both the RSC and GSC are required to develop different functions in the overall operation of the wind turbine. The RSC drives the wind turbine to achieve optimum power efficiency in winds below rated, to limit the output power to the rated value in winds above rated, or to adjust the active and reactive powers to the power references when power regulation is demanded [45,51]. The GSC is responsible for exchanging active power from the RSC and ESS, when it exists, to grid, and for exchanging reactive power when the operation with a defined power factor is required [45,51]. Moreover, the active power exchange with the battery can cause fluctuations in the DC bus voltage, which must be stabilized by a proper control strategy, as described later on.

4. Modeling of the ESS

The ESS consists of an electrochemical battery connected to the DFIG DC bus by a bidirectional DC/DC power converter. The modeling of both devices is described below.

4.1. Battery

The electrochemical lead-acid battery was modeled by using the model available in SimPowerSystems® [48]. It comprises a variable voltage source in series with an equivalent internal resistance. The model implemented calculates the magnitude of the voltage source as a function of the design parameters of the battery and its operating conditions.

In order to avoid internal damage of this device, it is crucial to maintain its SOC within certain recommended limits. Therefore, a supervisory control system was developed to control this parameter. This supervisory control acts on the battery power reference, avoiding the SOC to drop below 30% or to exceed 70%.

Characteristic parameters of the battery were selected from a commercial device, Discover's D21000, which is specially designed for renewable energy applications [52]. The battery was sized in terms of minimum capacity, so that its maximum instantaneous power is limited by the power of GSC. Connecting cells in series and parallel, a 585 Ah, 624 V battery was accomplished. Fig. 2 shows the discharge curve of the battery provided by the manufacturer and that obtained from the model implemented in this work. As can be seen, the agreement is quite acceptable.

4.2. DC/DC converter

A bidirectional DC/DC converter connects the battery to the DC bus. It allows the active power flow to/from the battery, enabling the charge and discharge of the device. The converter consists of a high frequency inductor, an output filtering capacitor, and two electronic IGBT-diode switches [53,54]. This converter can be controlled to accomplish either a stable DC bus voltage close to its reference, or a specified battery power flow set by the supervisory control system, as will be detailed in Section 5.

5. Control systems of the wind turbine and ESS

Three different control strategies are compared in this paper. One of them, named $C1$, is used to operate the DFIG wind turbine without battery. The other two, denoted as $C2$ and $C3$, were

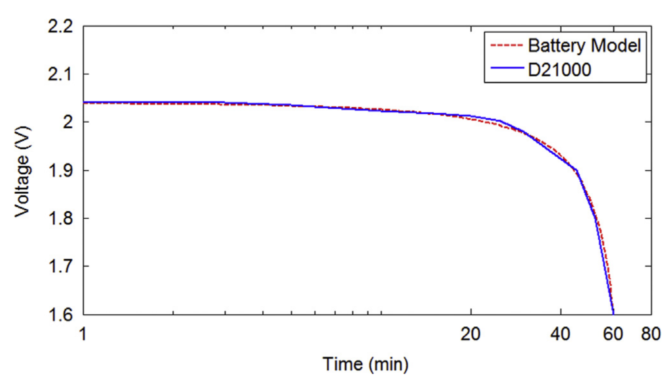


Fig. 2. Discharge curves for the commercial and modeled battery.

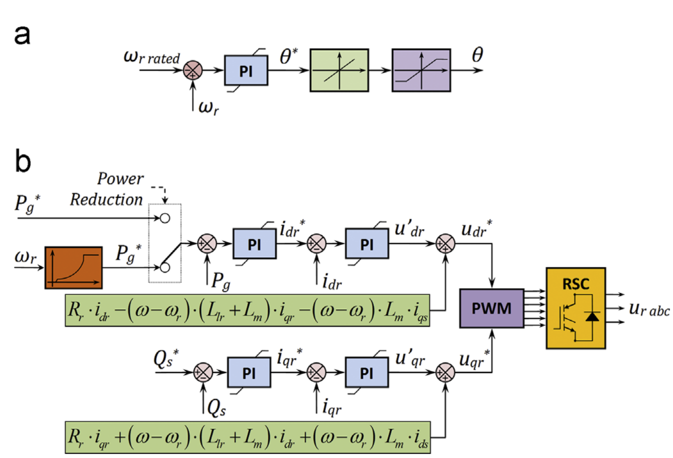


Fig. 3. (a) Pitch angle control scheme and (b) RSC control scheme.

implemented to accomplish a proper control of the hybrid wind turbine with battery.

The control strategy *C*1 is composed of three controllers (pitch angle, RSC and GSC controller), which interact to achieve the optimum efficiency operation of the DFIG wind turbine. However, the control strategies *C*2 and *C*3 require an additional controller (battery power converter controller) to drive the DC/DC power converter that connects the battery to the DFIG DC bus.

These controllers are described in detail below for each control strategy. Nonetheless, the pitch angle and RSC controllers are only described in detail for the control *C*1, since they are common for the three control strategies studied.

5.1. Control strategy C1

This control strategy, developed for the wind turbine configuration based on DFIG without battery, drives the wind turbine to achieve the optimum power efficiency in winds below rated, to limit the output power to the rated value in winds above rated, or to adjust the active and reactive powers to the power references when power regulation is demanded. Three controllers are needed to accomplish this behavior, which are described herein.

- Pitch angle control
  The pitch angle controller adjusts the blade pitch angle reducing the power coefficient, and thus, the aerodynamic power extracted from the wind, when the rotational speed increases up to the rated speed. The controller keeps the optimal pitch angle when the rotational speed remains below rated, and thus, the wind turbine operates with optimum power efficiency. On the other hand, when the wind turbine operates with power limitation or power reduction strategies, the pitch angle controller limits the rotational speed to the rated speed. In fact, this controller acts as a rotational speed limiter in any operating conditions [45]. The control scheme implemented is shown in Fig. 3a. The controller includes rate and angle limiters for the pitch angle movement.
- RSC control
  Vector control implemented in the RSC allows the decoupled control of the active and reactive power generation by acting on the *d* and *q* components of the rotor voltage, respectively. This controller presents the control scheme shown in Fig. 3b.
  In the reference frame chosen, the *d*-axis is oriented along the stator voltage vector, and thus, the *q* component of the stator voltage is zero. Combining Eqs. (1)–(4) and neglecting the stator winding resistance, the *d*–*q* components of the rotor voltage can be expressed as follows:

$$u_{dr} = R_r \cdot i_{dr} - (\omega - \omega_r) \cdot L_r \cdot i_{qr} - (\omega - \omega_r) \cdot L_m \cdot i_{qs} + u'_{dr} \quad (5)$$

$$u_{qr} = R_r \cdot i_{qr} + (\omega - \omega_r) \cdot L_r \cdot i_{dr} + (\omega - \omega_r) \cdot L_m \cdot i_{ds} + u'_{qr} \quad (6)$$

where u'_{dr} and u'_{qr} can be expressed as a function of i_{dr} and i_{qr}, respectively.

On the other hand, the total active power generated by the DFIG (P_g) can be calculated as the sum of the power provided by the stator (P_s), and the power flowing through the rotor windings (P_r). In fact, these three powers are expressed as follows:

$$P_s = 1.5 \cdot (u_{ds} \cdot i_{ds} + u_{qs} \cdot i_{qs}) \quad (7)$$

$$P_r = 1.5 \cdot (u_{dr} \cdot i_{dr} + u_{qr} \cdot i_{qr}) \quad (8)$$

$$P_g = P_s + P_r \quad (9)$$

Subsequently, when Eqs. (1)–(4) and (7)–(9) are combined and the stator resistance neglected, it is obtained that the total active power can be expressed as directly dependent on the *d* component of the rotor current, and therefore on the *d* component of the rotor voltage, as deduced from Eq. (5).

As seen in Fig. 3b, the RSC controller presents a selector to choose the operating mode that sets the active power reference. This selector is driven by a switching signal named *power reduction*. This signal is provided by the supervisory control system of the hybrid system, and it is automatically activated when the active power demand decreases below optimal generation in the configuration without battery. Then, two optional operating modes can be selected: power optimization/limitation and power reduction.

In the power optimization/limitation mode, the RSC controller uses the power–speed curve to define the active power reference according to the actual rotational speed. As a consequence, the wind turbine can operate with variable speed maximizing the power extracted from the wind in winds below rated or limiting the output power to rated power in winds above rated. In the power reduction mode, the controller uses the value ordered by the supervisory control system as a power reference, instead of the power reference derived from the power–speed curve.

The RSC controller is also responsible for regulating the reactive power flowing through the stator windings (Q_s). The stator reactive power depends on the *d*–*q* components of stator voltage and current

$$Q_s = 1.5 \cdot (u_{qs} \cdot i_{ds} - u_{ds} \cdot i_{qs}) \quad (10)$$

Combining Eqs. (1)–(4) and (10), and neglecting the stator windings resistance, it is obtained that the stator reactive power can be expressed as directly dependent on the *q* component of the rotor current. As deduced from Eq. (6), the *q* component of the rotor voltage u_{qr} can be expressed as directly dependent on the *q* component of the rotor current, and thus, the desired stator reactive power can be controlled by acting on the quadrature component of the rotor voltage.

As seen in Fig. 3b, once the rotor voltage references (u_{dr} and u_{qr}) are generated, a PWM generator provides a six-component vector containing the duty cycles of the IGBT switches included in the RSC. Finally, the magnitude of the three-phase rotor voltage injected to the rotor windings u_{rabc} is obtained.
- GSC control
  In the GSC, a similar control scheme has been used. In this case, the DFIG DC bus voltage and the reactive power flowing through the converter can be independently controlled by acting on the *d* and *q* components of the voltage at the grid side of the converter. This voltage can be expressed as follows:

$$u_{dg} = u_{ds} - R_{RL} \cdot i_{dg} + \omega \cdot L_{RL} \cdot i_{qg} - u'_{dg} \quad (11)$$

$$u_{qg} = u_{qs} - R_{RL} \cdot i_{qg} - \omega \cdot L_{RL} \cdot i_{dg} - u'_{qg} \quad (12)$$

where u_{dqg} represents the AC voltage at the grid side of the converter, R_{RL} and L_{RL} are the components of the impedance of the filter between the GSC and the grid, and i_{dqg} is the current flowing through the converter.

The voltages u'_{dg} and u'_{qg} can be expressed as a function of i_{dg} and i_{qg}, respectively. Hence, the u_{dqg} reference is generated by PI controller-based control loops, according to the control scheme shown in Fig. 4a.

Appling the power balance in the DC bus capacitor, it is obtained that the voltage at the DC bus can be expressed as a function of the RSC, GSC and battery – when it exists – power.

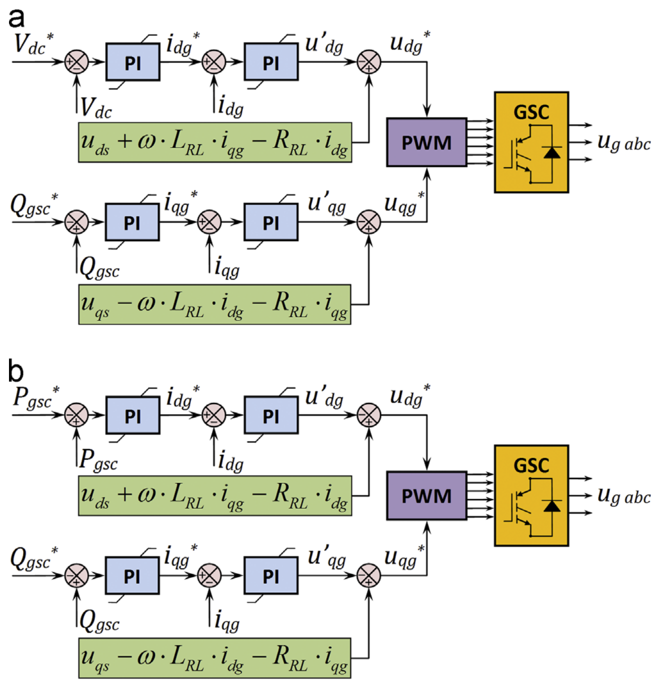


Fig. 4. (a) GSC control scheme used in the control strategy C1 and (b) GSC control scheme used in the control strategy C2.

$$P_r + P_{batt} - P_{gsc} = C \cdot \frac{dU_c}{dt} \cdot V_{dc} \tag{13}$$

where U_c is the capacitor voltage.

In case of the control strategy C1, the absence of ESS connected to the DC bus implies that the battery power P_{batt} is zero in Eq. (13).

On the other hand, the active power flow through the GSC is given by

$$P_{gsc} = 1.5 \cdot (u_{dg} \cdot i_{dg} + u_{qg} \cdot i_{qg}) \tag{14}$$

As previously stated, the *d*-axis of the reference frame is oriented along the grid voltage vector. Then, P_{gsc} can be expressed as directly dependent on u_{dg}, as deduced from Eqs. (11) and (14). As deduced from Eq. (13), the DC bus voltage can be controlled by regulating the active power flow through the GSC, since the rotor power depends on the operating conditions of the DFIG and the battery power is controlled depending on the power reference set by the supervisory control system – being zero for control strategy C1. Therefore, the DC bus voltage is controlled by acting on the component u_{dg}, as shown in Fig. 4a.

The reactive power transferred from/to the grid through the GSC can be expressed as

$$Q_{gsc} = 1.5 \cdot (u_{qg} \cdot i_{dg} - u_{dg} \cdot i_{qg}) \tag{15}$$

This reactive power depends directly on i_{qg}, and thus, on u_{qg}. As a result, the GSC reactive power is controlled by acting on the component u_{qg}, according to the control scheme shown in Fig. 4a. The reactive power reference Q^*_{gsc} is defined from the difference between the grid reactive power demand and the reactive power provided by the stator windings Q_s. It allows the DFIG wind turbine to operate with the demanded power factor. Finally, once the voltage references are generated, a PWM generator provides the duty cycles of the IGBT switches included in the GSC, and then, the magnitude of the three-phase grid side voltage u_{gabc} is obtained.

5.2. Control strategy C2

The control strategy C2, implemented for the hybrid wind turbine – battery system, is responsible for the combined operation of the DFIG and the storage device. Basically, it pursues the proper power management of DFIG and battery, while stabilizing the voltage at the DFIG DC bus and grid connection point.

The control C2 is composed of four controllers, one for each power converter (RSC, GSC and battery converter) and the pitch angle controller. The pitch angle and RSC controller are the same as those proposed for C1, and therefore, they are not described here. The GSC and battery power converter controller are explained next.

- GSC control
  In this case, the active and reactive powers delivered to grid through the GSC are controlled by acting on the *d* and *q* components of the voltage at the grid side of the converter. Fig. 4b shows the control scheme used for the GSC.
  As mentioned previously, P_{gsc} can be expressed as directly dependent on u_{dg}. As seen in Fig. 4b, the control loop developed for u_{dg} adjusts the GSC active power to the power reference P^*_{gsc}. This power reference is calculated from the difference between the rotor active power P_r and the active power to be stored in or provided by the battery, which is defined by the supervisory control system.
  As previously stated, the *q* component of the voltage at the grid side of the converter regulates the reactive power that the GSC exchanges with the grid. Thus, the control scheme for Q_{gsc} is similar to that used in the control strategy C1.
  Once the u_{dg} and u_{qg} references are calculated, a PWM generator drives the IGBT switches in the GSC to generate the three-phase voltage at the grid side of the converter u_{gabc}.
- Battery power converter control
  In the control strategy C2, the control system of the battery power converter has been designed in order to maintain the DFIG DC bus voltage close to its nominal value (1150 V).

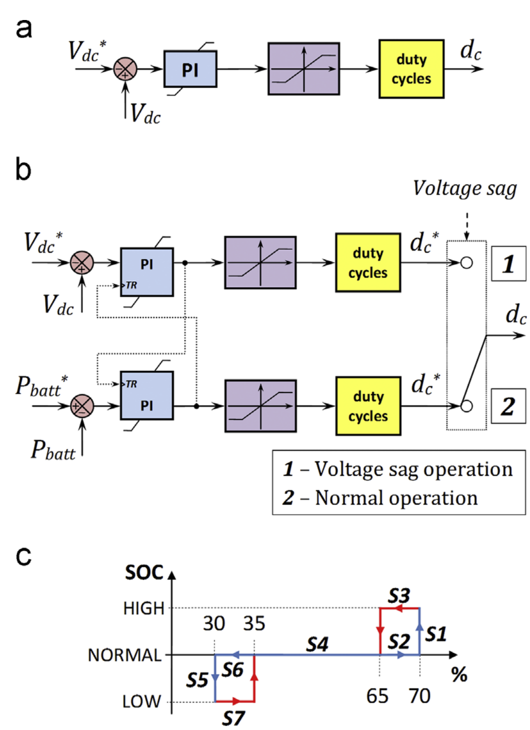


Fig. 5. (a) Battery power converter control scheme used in configuration C2; (b) Battery power converter control scheme used in configuration C3; and (c) Hysteresis cycles for the levels battery SOC.

A single PI controller-based control loop compares the DC voltage reference with the actual DC voltage measurement and defines the duty cycle for the IGBT switches of the battery power converter. This control is illustrated in Fig. 5a.
This controller stabilizes the DC bus voltage when the power flow through the DFIG DC link between RSC and GSC varies, thus allowing the charge and discharge of the battery when possible.

5.3. Control strategy C3

This control strategy is a variant of the control strategy *C*1, which allows the combined operation of the DFIG wind turbine and battery as ESS. In fact, the control schemes implemented for the RSC, GSC, and pitch angle controller are the same as those used in the control strategy *C*1. In this section, the control implemented for the battery power converter is explained, which differs from that implemented in the control strategy *C*2.

- Battery power converter control
In the control strategy *C*3, the battery power converter controller presents a selector for the choice of control scheme, depending on the operating mode of the hybrid system.
Whenever no grid voltage contingencies happen (normal operation), the battery power converter is controlled to manage the active power flow from the battery to the DFIG power converter. Therefore, the battery will be charged and discharged by absorbing or providing active power to the DC bus, respectively. It can be accomplished with a single control loop based on a PI controller, as shown in Fig. 5b. The battery power reference set by the supervisory control system is compared with the actual measurement. A PI controller uses this error signal to define the duty cycle that drives the IGBT switches of the converter.
On the other hand, under voltage sags operation, the battery is used to stabilize the voltage at the DFIG DC bus, thus enabling a faster recovery of the whole system after the fault clearance. As shown in Fig. 5b, a control scheme similar to that presented for the control strategy *C*2 operates transitorily. It uses a PI-based control loop to regulate the DC bus voltage to its rated value.
Since both PI controllers will not be active at the same time, transitory disturbances may appear when switching the selector. To achieve a smooth transition between these control schemes, a lead-track layout has been developed, in which the output of each PI controller is connected to the tracking input of the other, as observed in Fig. 5b.

6. Supervisory control system

The hybrid system requires a supervisory control system that coordinates the performance of both energy sources (DFIG wind turbine and battery) and allows a reliable and controlled response. In this work, a state machine-based control system has been developed in order to achieve the coordinate operation of the wind turbine and battery.

This supervisory control sets the power reference to be provided by/stored in the battery, depending on its SOC and the power mismatch between the power generated by the DFIG (P_g) and the power demanded by the grid (P_{demand}). Moreover, it activates the power reduction mode when the battery reaches its maximum SOC, and forces the battery charge when the SOC achieves the minimum level. Nevertheless, the battery will be controlled to supply the demanded power whenever the SOC is within the secure operation range (from 30% to 70% of the total capacity).

The supervisory control system has been implemented by using a truth table block. It presents three input signals, i.e. the power mismatch, the battery SOC, and the power generated or consumed through the rotor windings (P_r). Two internal variables, named *Low_SOC* and *High_SOC*, are used to implement a 5% SOC hysteresis for the minimum and maximum limits. Finally, the output signals are the battery power reference and the switching signal *power reduction*, which indicates when this operating mode must be applied.

Seven different states depending on the battery SOC are considered. Changes between the SOC levels are performed according to Fig. 5c, where two hysteresis cycles for the control of the level changes are shown. It avoids constant switching between bordering states.

In the implemented truth table, each state is defined by a condition. As a consequence, when a specific condition is found true, a certain action is generated, and the subsequent instruction is executed. The description of the states and corresponding actions is given as follows.

- **State** 1: $SOC \geq 70\% \rightarrow Action$ 1. When the battery reaches its maximum recommended SOC, both the internal variable *High_SOC* and the switching signal *power reduction* are forced to 1. Then, the active power reference will not be set as a function of the angular velocity, but as a predetermined value given by the power demand, avoiding the active power generation to exceed the demand. In addition, the battery power reference will be set to the minimum value between zero and *power unbalance*, thus allowing the discharge when *power unbalance* is negative.
- **State** 2: $SOC \geq 65\%$ *and* $High_SOC = 0 \rightarrow Action$ 2. In this state, since the battery has not reached its maximum SOC, the output *power reduction* is not active. Hence, the RSC control operates with the optimization/limitation strategy. Because either battery charge or discharge is allowed, the battery power reference will be set to compensate the power mismatch between generation and demand by using the *power unbalance*.
- **State** 3: $SOC \geq 65\%$ *and* $High_SOC = 1 \rightarrow Action$ 3. In this case, the *power reduction* mode is active, and only the battery discharge is feasible. Therefore, the battery power reference is set to the minimum value between zero and *power unbalance*.
- **State** 4: $35\% \leq SOC \leq 65\% \rightarrow Action$ 4. When the SOC varies within this range, it is considered that the battery operates with normal SOC, and no restrictions are applied. Both internal variables *High_SOC* and *Low_SOC* are set to 0. The wind turbine operates in the optimization/limitation mode, and the battery compensates the *power unbalance*.
- **State** 5: $SOC \leq 30\% \rightarrow Action$ 5. If the SOC decreases below this minimum recommended value, internal damage can happen inside the device. Therefore, deeper discharge is avoided by setting the internal variable *Low_SOC* to 1. In addition, the battery is forced to recharge, since its power reference will be the maximum value between *power unbalance* and the absolute value of the rotor active power (P_r).
- **State** 6: $SOC \leq 35\%$ *and* $Low_SOC = 0 \rightarrow Action$ 6. In this state, the battery has not reached its lowest SOC. Hence, either battery charge or discharge is allowed. As a consequence, the battery power reference will be set to compensate the *power unbalance*.
- **State** 7: $SOC \leq 35\%$ *and* $Low_SOC = 1 \rightarrow Action$ 7. When the battery has been discharged to its minimum recommended limit, the recharging process must take place at least until the SOC exceeds 35%. Therefore, the battery power reference defined in *State* 5 is also valid in *State* 7. It avoids damaging the storage device and guarantees an adequate recovery of the battery capacity.

Table 1 summarizes the control strategy developed for the supervisory control system. The acronym NM stands for Not Modified when the variable value does not change in certain state.

Table 1
Summary of the supervisory control system.

State/ action	High_SOC	Low_SOC	Power reduction	P_{batt}
A1	*1*	*NM*	1	*Min*(0, *power unbalance*)
A2	*NM*	*NM*	0	*Power unbalance*
A3	*NM*	*NM*	1	*Min*(0, *power unbalance*)
A4	*0*	*0*	0	*Power unbalance*
A5	*NM*	*1*	0	*Max*(P_r, *power unbalance*)
A6	*NM*	*NM*	0	*Power unbalance*
A7	*NM*	*NM*	0	*Max*(P_r, *power unbalance*)

7. Simulation results and discussion

The dynamic responses of the wind turbine configurations and the control schemes previously described were compared under different working conditions. Five simulations were carried out, in which the main features of the wind power systems were evaluated.

The first simulation shows a long term performance under measured fluctuating wind speed that varies both above and below rated speed. In addition, the active and reactive power references also change along the simulation as the grid demand varies. This simulation is carried out to show the suitable performance of the three wind power systems, and the improvements that hybrid wind turbine presents under normal operation, with variable wind speed and grid demand. The following simulations consider the response of the three wind power systems to various grid faults. In these cases, the main aim is to study the improvements that the hybrid wind turbine presents under power grid contingencies. Constant wind speed is considered in order to avoid power fluctuations due to variable wind effects.

In the subsequent figures that show the results obtained in the simulations, the wind turbine configurations are denoted as follows: *C*1 (DFIG wind turbine with control strategy 1); *C*2 (hybrid wind turbine, DFIG and battery, with control strategy 2); and *C*3 (hybrid wind turbine, DFIG and battery, with control strategy 3).

7.1. Case 1: variable wind speed and grid demand

In the performed simulation, the active power demanded by the grid varies along the simulation. The active power demand is set to 0.9 pu during the first 60 s. At 60 s, the active power demand increases, with a rising slope of 0.1 pu/s, until it reaches 1 pu. This demand is kept until 180 s. Then, the demand increases up to 1.1 pu, which is maintained for the rest of the simulation. Moreover, the reactive power references for stator and GSC are also variable, achieving a total reactive power generation that ranges in four different levels between 0 and 0.5 pu of 60 s duration each.

The wind speed profile used in the first case-study is shown in Fig. 6a. This wind speed series has been extracted from real measurements in Tarifa (Spain) for the 6th of December, 2013 [55]. The wind speed remains mostly above its rated value during the first 115 s, while it fluctuates below rated for the rest of the simulation.

As seen in Fig. 6b, the rotor angular speed varies above the rated speed (1.2 pu) for winds above rated (during the first 115 s), since the blade pitch controller acts on the pitch angle to limit the power extracted from the wind, and subsequently, the rotor speed. For winds below rated, the rotor speed varies accordingly to the wind speed changes, since the blade pitch angle is set to the minimum value in order to maximize the power extracted from the wind. It is remarkable that no differences can be observed between the responses of configurations *C*2 and *C*3, which implement the wind turbine with battery. Nonetheless, the absence of ESS in configuration *C*1 implies that the DFIG must reduce power generation in order to address the grid power demand during a period involving the first 60 s approximately. Hence, configuration *C*1 operates in the power reduction mode, increasing the blade pitch angle to reduce the power captured from the wind, as shown in Fig. 6 c. On the other hand, configurations *C*2 and *C*3 operate in the optimization/limitation mode with maximum power capture efficiency, in which the active power surplus is stored in the battery, thus enabling a more efficient performance compared to configuration *C*1. After the first 60 s, the grid demand increases and configuration *C*1 adopts the optimization/limitation strategy.

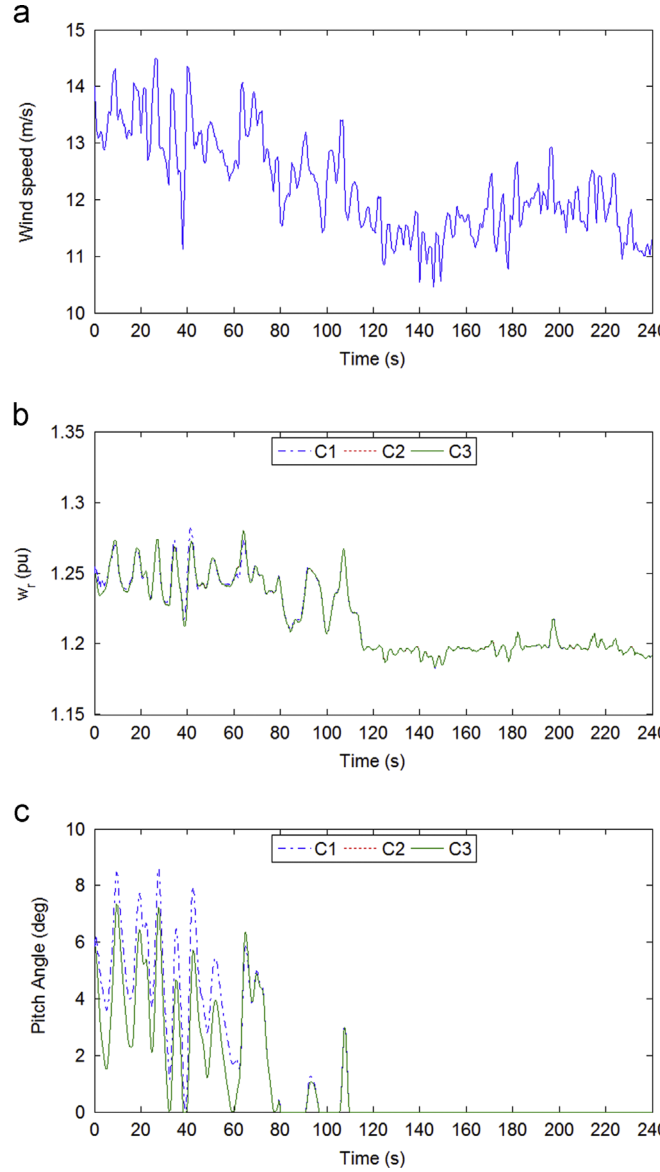


Fig. 6. (a) Wind speed profile; (b) rotor speed; and (c) pitch angle in Case 1.

Fig. 7a illustrates the total active power delivered to grid by the wind turbine (configuration *C*1) and hybrid wind turbines (configurations *C*2 and *C*3). It can be seen that, as long as the active power demand remains below optimum generation, configuration *C*1 switches to the power reduction mode in order to cover grid requirements, which leads to a decrease in the wind turbine efficiency, since significant amounts of wind power are wasted and not stored in an ESS. However, when above rated output

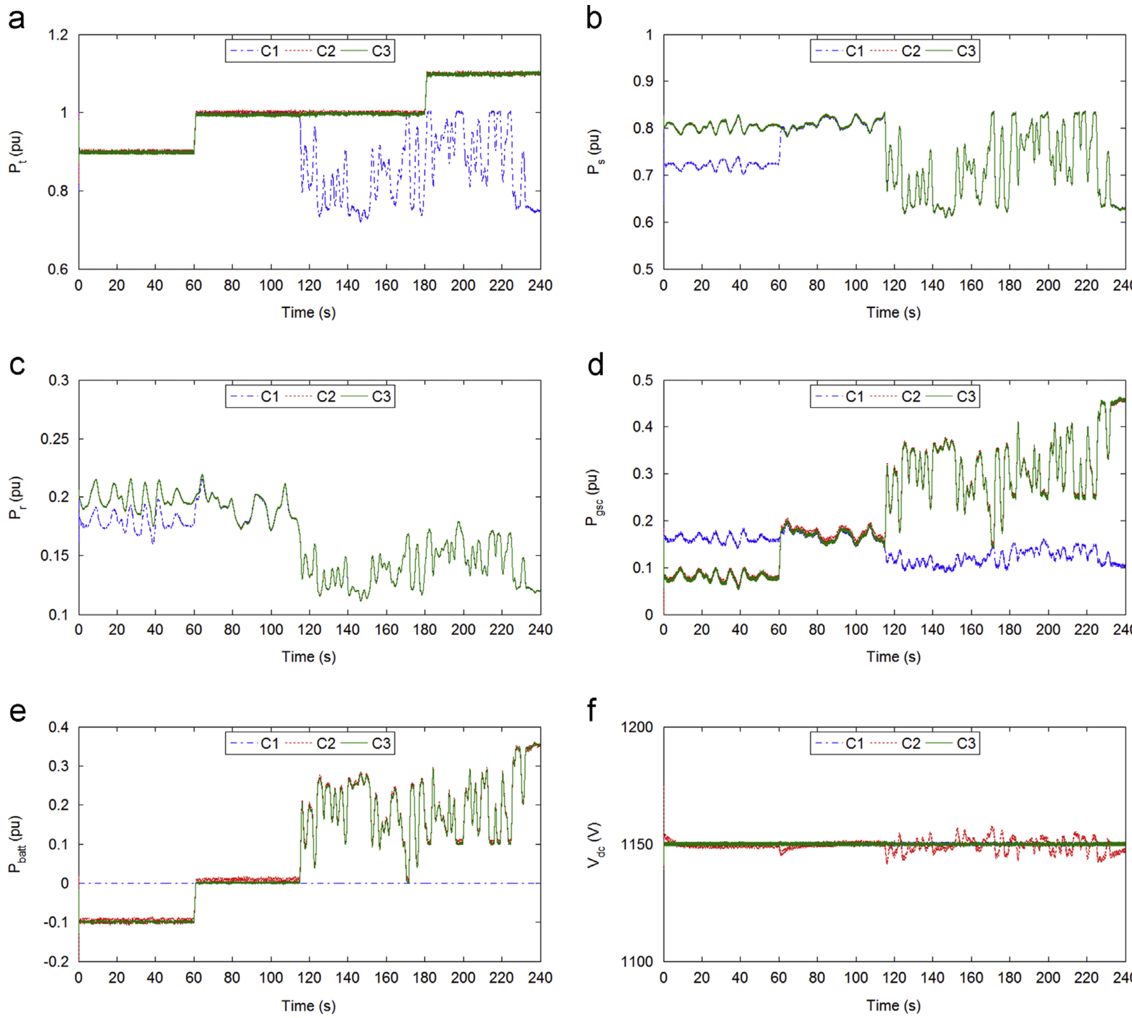


Fig. 7. (a) Total active power; (b) stator active power; (c) rotor active power; (d) GSC active power; (e) battery active power output; and (f) voltage at the DC bus of the DFIG in Case 1.

power is demanded, configuration *C*1 is not able to address the grid requirements, since it does not incorporate any ESS which supplements the wind turbine generation. On the other hand, the hybrid systems *C*2 and *C*3 adjust satisfactorily the generation to the grid demand changes either below or above the DFIG rated power, despite wind speed fluctuations. Therefore, configurations *C*2 and *C*3 allow decoupling the power generation and demand by using the battery as an active ESS whenever it is needed. These differences are also illustrated in Fig. 7b. As seen, configurations *C*2 and *C*3 present the same active power flow through the stator windings during all simulation time. However, configuration *C*1 provides a lower power when the power reduction mode is active (during the first 60 s approximately), and reaches the optimal value soon after the RSC controller switches to the optimization/limitation control strategy.

The active power flow through the rotor windings shows an analogous response to that observed for the stator active power, as seen in Fig. 7c. Hence, configuration *C*1 presents lower rotor active power while operating in the power reduction mode. Nevertheless, the three configurations show similar rotor active power when they adopt the optimization/limitation control strategy.

Since the RSC controller regulates the total active power generated by the wind turbine (sum of stator and rotor active powers), the GSC active power flow will not be affected by the power reduction applied to configuration *C*1 during the first 60 s, as seen in Fig. 7d. For the rest of simulation, the GSC active power provided by configuration *C*1 follows the optimal generation curve as a function of wind speed. On the contrary, the connection of an ESS in the DC bus of the DFIG, in case of configurations *C*2 and *C*3, modifies the power flow through the GSC. In fact, the GSC active power of configurations *C*2 and *C*3 remains below that provided by configuration *C*1 when power is being stored in the battery (from 0 to 60 s approximately), whereas the opposite occurs when the battery provides power to the grid (between 115 s up to the end of the simulation), since the battery power is delivered to grid through the GSC.

The battery active power response is depicted in Fig. 7e. For configurations *C*2 and *C*3, a negative value close to -0.1 pu can be observed during the battery energy storage. On the other hand, as long as the active power demand remains equal to the rated generation, the battery does not store or provide active power. Finally, from 115 s on, the battery delivers active power in order to address the grid demand in configurations *C*2 and *C*3. In case of configuration *C*1, the battery active power is zero, because it works without a battery.

Fig. 7f shows the DC bus voltage at the DFIG. As seen, configuration *C*2 experiences slight deviations on the DC bus voltage when the battery active power flow varies considerably. Nevertheless, this parameter is always satisfactorily controlled close to its reference, since the maximum variations do not exceed 1% of the nominal voltage. For configurations *C*1 and *C*3, the DC bus voltage remains stable at its reference.

Wind turbines equipped with DFIG allow a decoupled control of active and reactive power generation. In this simulation, a variable reactive power grid demand has been set for the wind turbine. Therefore, the generator must be able to regulate the reactive power flow through the stator windings and the GSC in order to address the grid requirements. Fig. 8a shows the total reactive power output from the wind turbine. As seen, four different levels have been accomplished. Moreover, no noticeable differences exist between the three configurations developed, since the battery is not responsible for providing reactive power in any case.

The reactive power supplied by the stator windings is shown in Fig. 8b. Its reference remains stable at 0.2 pu during the time interval ranging from 60 s to 180 s, and zero for the rest of the simulation. The GSC must provide the difference between the total reactive power demand and the stator generation, as illustrated in Fig. 8 c. As a result, the converter delivers 0.3 pu during the first 120 s of the simulation.

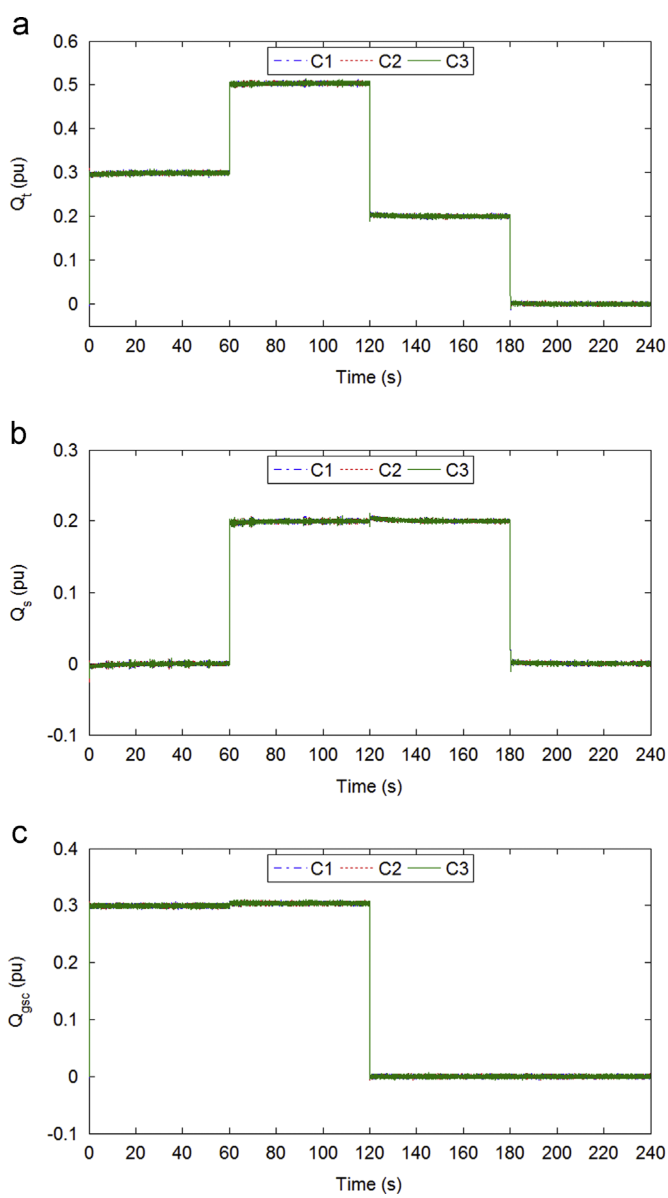


Fig. 8. (a) Total reactive power; (b) stator reactive power; and (c) GSC reactive power in Case 1.

7.2. Case 2: voltage sag

A ten seconds-long simulation was carried out in order to check the response of the wind turbine configurations implemented when a voltage sag occurs at the grid connection point. The fault consists of a voltage drop to 0.2 pu at the point of common coupling to grid at time 2 s. Then, the voltage recovers to 1 pu at 2.4 s. During the simulation, the wind speed is assumed constant below rated at 11 m/s.

Wind turbines are required not to disconnect from grid as long as the voltage sag remains within certain specified voltage and time limits. Moreover, active and reactive power supply to the grid is a crucial factor to ride through grid voltage sags. In this simulation, up to the appearance of the fault, the three configurations operate at optimal generation, and the ESS – when exists – does not absorb or provide considerable amounts of power. During the voltage sag, a positive output reference has been set for both active and reactive power, in order to help in grid recovery. Finally, right after the fault clearance, the optimal generation reference is set again, and the power output must recover its previous value. Fig. 9a shows the total active power output of the wind turbine. It reveals that configuration *C*1 drastically reduces its active power supply to the grid during the voltage sag up to 0.17 pu approximately. On the contrary, configurations *C*2 and *C*3 allow an extra support due to the battery contribution. Regarding configuration *C*3, a value of 0.195 pu is registered at the end of the fault. On the other hand, configuration *C*2 presents its highest value at 0.35 pu, which is 80% (106%) higher than that achieved by configuration *C*3 (*C*1). In addition, configuration *C*2 shows a faster recovery of steady state compared to configurations *C*1 and *C*3.

During the grid fault, configuration *C*2 extracts more power from the battery than configuration *C*3 (Fig. 9b), which leads to a higher total active power output to the grid. When the voltage sag is cleared, configurations *C*2 and *C*3 use the battery to store energy, which accelerates the stabilization of the total active power output. The absence of an ESS in configuration *C*1 causes a slower recovery of the steady state.

The total reactive power supply is represented in Fig. 9c. As said before, only during the voltage sag a positive reactive power reference was set for the three configurations. Initially, after a short transitory, configuration *C*2 shows a slightly higher reactive power injection. Nonetheless, towards the end of the fault, no remarkable differences can be appreciated between the three configurations.

Finally, Fig. 9d shows the DC bus voltage. As seen, this parameter is controlled close to its reference in the three configurations. A maximum instantaneous deviation of 6% below rated value is found in configuration *C*2. Nevertheless, this perturbation does not affect the proper operation of the wind turbine, nor implies risk of damage for the electric equipment.

A sensitivity study of this fault has been carried out for the PI controllers implemented on the active power and DC voltage control schemes in Figs. 4 and 5. Hence, four signals have been evaluated: (a) P_{gsc} for *C*2; (b) V_{dc} for *C*1; (c) P_{batt} for *C*3; and (d) V_{dc} for *C*2. Their response to the 0.2 pu voltage sag is shown in Fig. 10a–d for different values of the proportional (k_p) and integral (k_i) gains in the PI controllers. In all cases, the red line illustrates the values used in the models presented in this paper, whereas the blue and green lines correspond to the sensitivity study.

In Fig. 10a, it can be observed that increasing the integral term of the controller four orders of magnitude above the proportional, still allows controlling the reference signal P_{gsc}. Nonetheless, flicker at the end of the fault appears as the difference between both gains grows. On the other hand, when both terms are in a similar order of magnitude, the controlled parameter becomes oscillating, thus not being adequate gain values for this purpose.

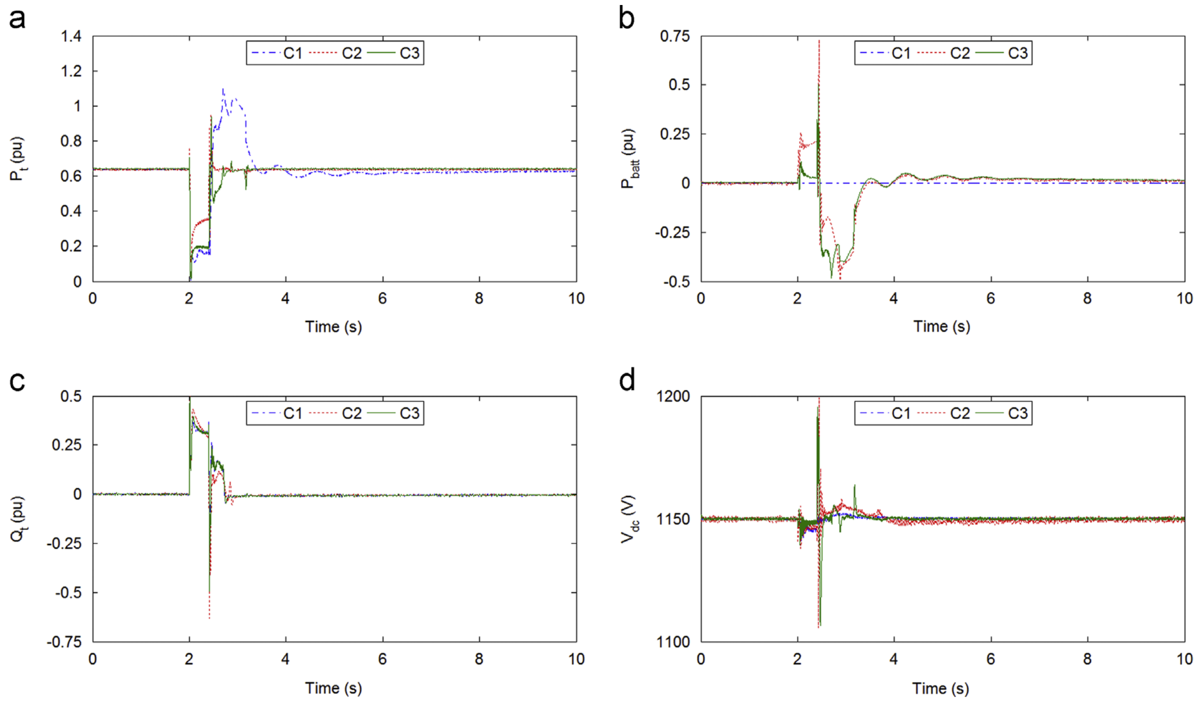


Fig. 9. (a) Total active power output; (b) battery active power output; (c) total reactive power output; and (d) voltage at the DC bus of the DFIG in Case 2.

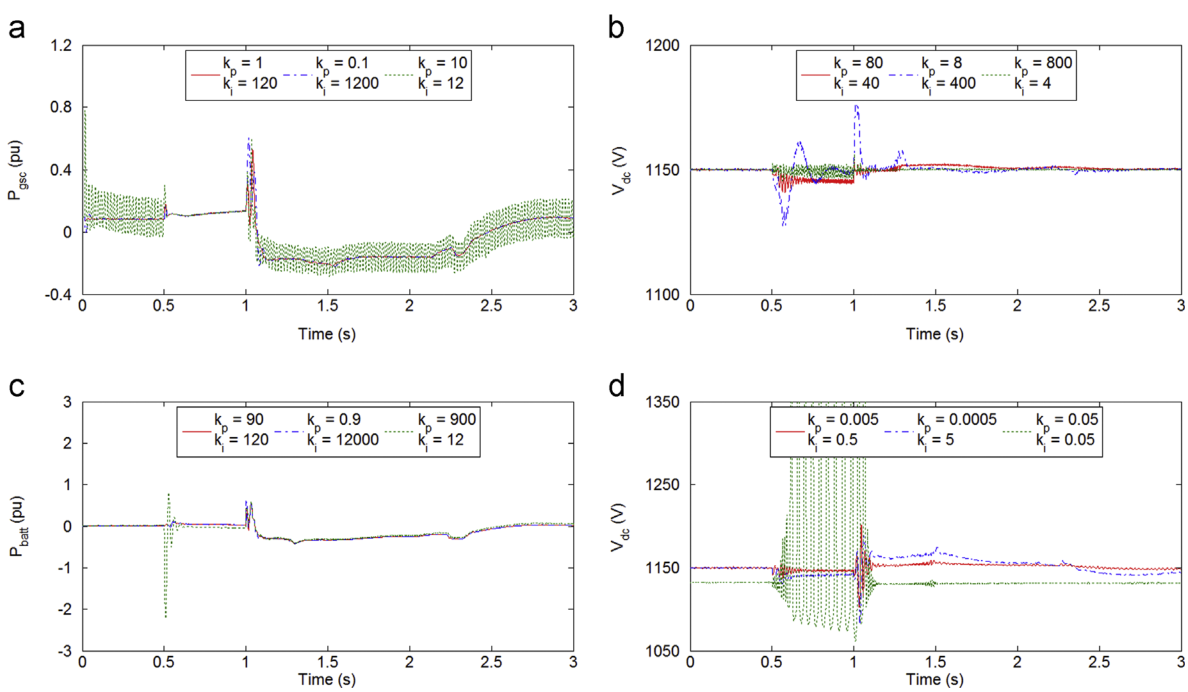


Fig. 10. (a) P_{gsc} for *C*2; (b) V_{dc} for *C*1; (c) P_{batt} for *C*3; and (d) V_{dc} for *C*2.

The DC bus voltage controller in configuration *C*1 is sensitivity-tested in Fig. 10b. As seen, larger fluctuation can be noticed for an integral gain two terms of magnitude above the proportional. On the other hand, when the proportional term becomes two orders of magnitude higher than the integral, these fluctuations become much faster and consistent during the fault, although with reduced amplitude. Therefore, the design values selected were of a similar order of magnitude for the proportional and integral gains.

For the battery active power controller in configuration *C*3 (Fig. 10c), proximal gain values were chosen, with the integral term slightly higher than the proportional. In the sensitivity analysis, it is noticed that this PI controller offers a wide range of acceptable variation for the gains. As seen in Fig. 10c, it is necessary to greatly increase the integral term above the proportional to observe fast oscillations during the recovery of the fault. On the other hand, only one order of magnitude higher for the proportional gain above the integral provokes noticeable fluctuations on the controlled signal at the detection of the voltage sag. Hence, this regulator improves its stability for higher values of integral gains compared to the proportional.

Regarding the DC bus voltage controller implemented on the DC/DC battery converter in configuration *C*2, it can be observed in

Fig. 10d that two orders of magnitude less are needed in the proportional term compared to the integral, being both gains below unity. When this difference grows, the signal can be still controlled, but the error recorded during the fault increases. Moreover, it takes longer for the controlled signal to regain its reference value after the fault is cleared. On the other hand, if the proportional and integral gains are of a similar order of magnitude, the response fluctuates uncontrolled during the voltage sag. Additionally, the controller becomes excessively slow and it is not able to reach the established reference value even in steady-state conditions.

In Fig. 11a and b, the total active power generation for control strategies *C*2 and *C*3 is compared for two additional voltage sags. These faults have a duration of 0.8 s and 1 s, with a voltage of 0.5 pu and 0.8 pu at the point of common coupling to grid, respectively, for Fig. 11a and b. As seen, *C*2 also outperforms *C*3 for these situations, achieving a higher active power injection to grid in all cases. Moreover, in the least severe fault of 0.8 pu (Fig. 11b), with the control strategy *C*2 it is possible to supply the grid with up to 1.23 pu active power generation of the hybrid system. This generation above the rated value improves the FRT of the power system, and offers additional compensation for potential disconnection of other power sources during the voltage sag.

7.3. Case 3: three-phase fault to ground

A three-phase fault to ground at the wind turbine output terminals was simulated in this case study. It was considered to happen at the low voltage side (575 V) of the transmission line at time 2 s, and cleared at 2.5 s. Also, a constant wind speed of 11 m/s was used as input for the wind turbine.

The proposed fault causes a sudden drop on the generator voltage, and subsequently on the total active power generation of the wind turbine and hybrid wind turbine schemes, as shown in Fig. 12a. It can be observed that again, the ESS allows configurations *C*2 and *C*3 to achieve stable operation notably faster than *C*1. During the fault, control *C*2 shows a slightly higher power injection, but the most remarkable improvement of this strategy arises at time 2.5 s when the fault is cleared. As seen, both *C*1 and *C*3 undergo a sharp transient that provokes an active power consumption of 0.37 pu for *C*3, despite the presence of an ESS; and 0.78 pu for *C*1. Control *C*2 does not consume active power from the grid during the recovery of the system, thus performing a softer and more reliable transition to steady state.

Regarding the DC bus voltage in Fig. 12b, an inadequate behavior was observed for *C*1. During the fault, this voltage decreases to 200 V, which is 17% of the nominal value for the DFIG DC bus, thus risking the proper operation of the generator. For control *C*3, a maximum value of 1300 V is registered after the fault clearance, whereas configuration *C*2 accomplishes better control of the DC bus voltage both during and after the fault, with a maximum difference of 50 V below the reference value during the transient recovery.

No relevant differences were observed for the reactive power and grid voltage response. Therefore, these parameters are not shown here.

7.4. Case 4: single-phase fault to ground

In this case study, the fault to ground was simulated in only one phase at the DFIG output terminals at time 2 s. The fault remains unsolved during 0.5 s. Additionally, a constant wind speed of 14 m/s is used, which falls above the rated value of the wind turbine.

The total active power response of the three configurations evaluated is illustrated in Fig. 13a. Contrarily to Case 3, now controls *C*2 and *C*3 achieve a notable extra active power injection during the fault (approximately a minimum value of 0.55 pu versus 0.2 pu registered for *C*1). However, it can be appreciated

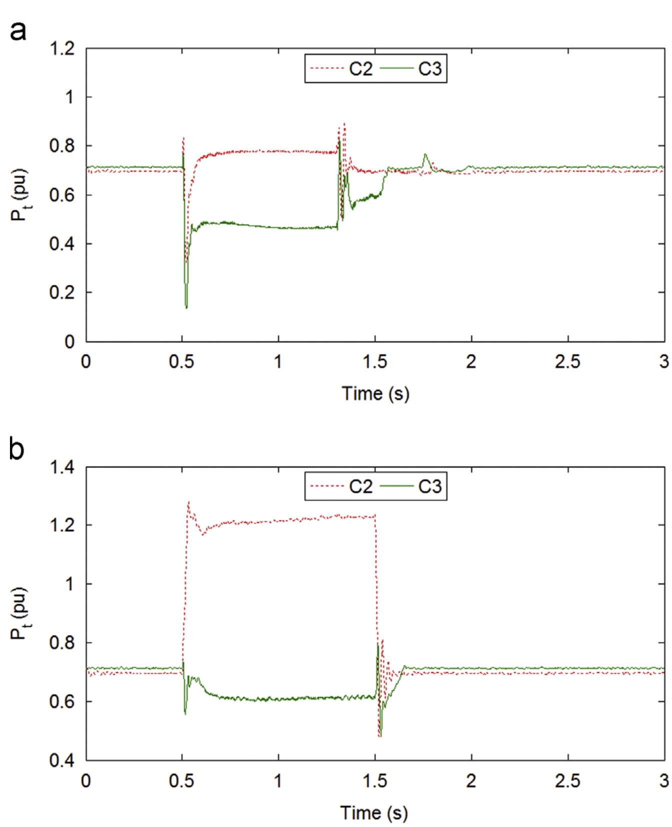


Fig. 11. (a) Voltage sag 0.5 pu–0.8 s and (b) voltage sag 0.8 pu–1 s.

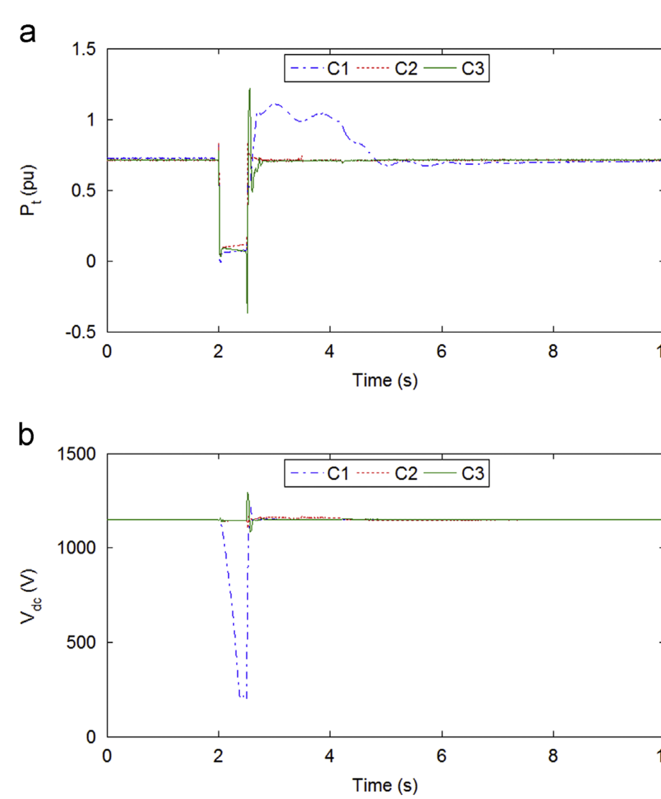


Fig. 12. (a) Total active power output and (b) voltage at the DC bus of the DFIG in Case 3.

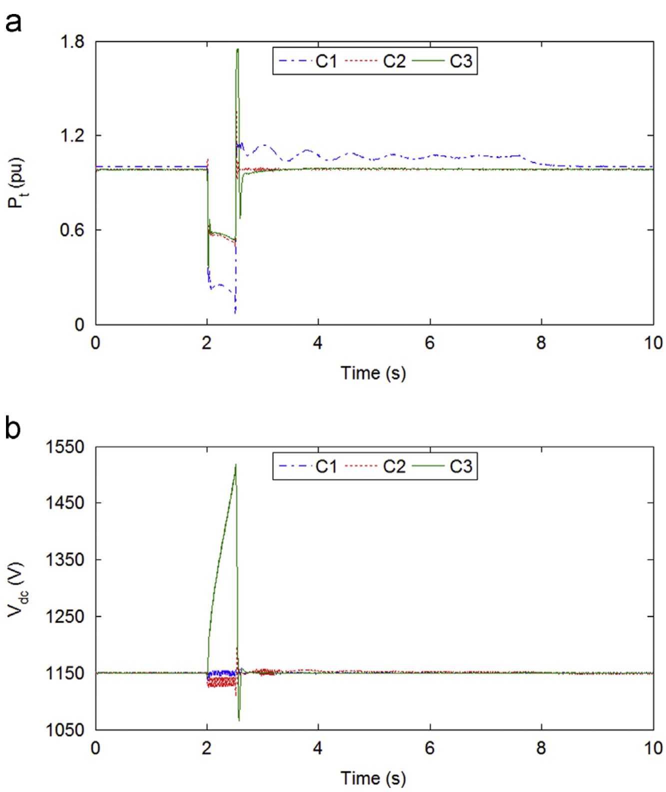


Fig. 13. (a) Total active power output and (b) voltage at the DC bus of the DFIG in Case 4.

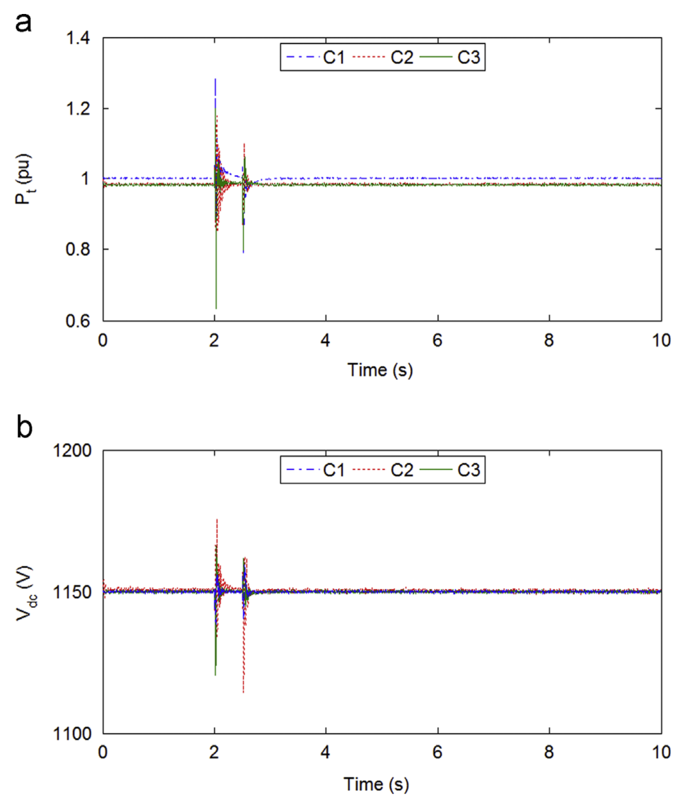


Fig. 14. (a) Total active power output and (b) voltage at the DC bus of the DFIG in Case 5.

that the control strategy *C*2 performs a better FRT, given the maximum peak of 1.75 pu active power generation recorded for *C*3 at 2.5 s. This sudden increment is not desirable. It does not contribute to the grid recovery after the fault, since the voltage has already regained its steady state conditions. Hence, a softer response as the one attained by *C*2 is more adequate. Also, the faster recovery of the hybrid systems after the fault clearance is evident in this simulation. Configuration *C*1 takes 5.5 s to reach steady state once the disturbance has been released, whereas *C*2 and *C*3 overcome short and quick transitory fluctuations.

Voltage at the DC bus is shown in Fig. 13b. As seen, configuration *C*3 increases above 1500 V by the end of the fault. This poses a dangerous situation for the DFIG and should be avoided. On the other hand, controls *C*1 and *C*2 are able to regulate the DC voltage close to its reference during and after the fault.

The reactive power and grid voltage response did not show remarkable differences between the control strategies presented, and thus they are not shown.

7.5. *Case 5: overvoltage*

Overvoltage at the point of common coupling of the systems to grid was evaluated. A voltage of 1.2 pu is measured from time 2 s to 2.5 s. This disturbance states different requirements for the wind turbine and hybrid wind turbines compared to the previous faults. Here, also constant wind speed of 14 m/s was considered.

Contrarily to voltage drops, the total active power generation does not decrease substantially during the fault (Fig. 14a). Therefore, the contribution of the ESS is less important than in the previous simulations. As a consequence, a similar performance is shown for the three control strategies. At the beginning of the fault, active power fluctuates rapidly, being this transient more accused for *C*3 (maximum peak of 1.2 pu and minimum of 0.65 pu), than for *C*2 (1.18 pu, 0.78 pu) and *C*1 (1.21 pu, 0.8 pu). Nevertheless, this transitory behavior is damped faster in strategies *C*1 and *C*3 compared to *C*2.

The DC bus voltage registers a similar response, with transitory fluctuations both at the beginning and after the clearance of the fault (Fig. 14b). However, despite these oscillations, the three configurations show adequate FRT capabilities to the overvoltage situation.

The representation of the reactive powers and grid voltage is omitted since no relevant differences between the control strategies were appreciated.

8. Conclusions

This paper presented a thorough comparative study of two different control strategies for DFIG wind turbines with batteries as ESS (namely *C*2 and *C*3) and the configuration of DFIG without batteries (namely *C*1). The main characteristics of the systems were described in detail. Vector control was employed to perform decoupled active and reactive power management, and DC bus voltage regulation in the DFIG, as well as in the DC/DC battery converter when necessary. Moreover, a supervisory control system was presented that allowed coordinated operation of the ESS and DFIG in the hybrid systems.

The configurations considered were tested under varied operating conditions. First, a variable active and reactive power grid demand simulation, with measured fluctuating incoming wind speed, showed the main benefits of incorporating an ESS to wind power generation. Hence, both hybrid systems were able to address grid demand, and attain constant power generation regardless of the wind speed; whereas *C*1 could only adapt to demand when it remained below or equal to the optimal generation according to wind speed. On the other hand, reactive power grid requirements were successfully fulfilled by the three configurations. Afterwards, FRT capabilities of the three

schemes were evaluated by simulation of four grid faults (voltage sag, three-phase fault to ground, single-phase fault to ground, and overvoltage). Control strategy *C*2 achieved better response to several faults with diverse characteristics and occurred at different points of the network. Therefore, results suggest that the control strategy *C*2 is a more suitable option than control *C*3 for hybrid wind turbines. Both alternatives present an adequate response under normal operation. However, the former reaches a better overall performance, thus improving the grid integration of wind turbines.

Acknowledgments

This work has been supported by the University of Cadiz under the Grant FPI 2012-036, by the Spanish Ministry of Science and Innovation under Grant ENE2010-19744/ALT, and by the Foundation Technological Campus of Algeciras.

References

[1] Panwar NL, Kaushik SC, Kothari S. Role of renewable energy sources in environmental protection: a review. Renew Sustain Energy Rev 2011;15:1513–24.
[2] Pullen A, Sawyer S, editors. Global wind report 2010. Brussels: Global Wind Energy Council ⟨http://www.gwec.net/index.php?id=180⟩ [accessed November 2011].
[3] Varun, Prakash R, Bhat IK. Energy, economics and environmental impacts of renewable energy systems. Renew Sustain Energy Rev 2009;13:2716–21.
[4] Mostafaeipour A. Productivity and development issues of global wind turbine industry. Renew Sustain Energy Rev 2010;14:1048–58.
[5] Evans A, Strezov V, Evans TJ. Assessment of sustainability indicators for renewable energy technologies. Renew Sustain Energy Rev 2009;13:1082–8.
[6] Haas R, Panzer C, Resch G, Ragwitz M, Reece G, Held A. A historical review of promotion strategies for electricity from renewable energy sources in EU countries. Renew Sustain Energy Rev 2011;15:1003–34.
[7] Saidur R, Rahim NA, Islam MR, Solangi KH. Environmental impact of wind energy. Renew Sustain Energy Rev 2011;15:2423–30.
[8] Welch JB, Venkateswaran A. The dual sustainability of wind energy. Renew Sustain Energy Rev 2009;13:1121–6.
[9] Beaudin M, Zareipour H, Schellenberglabe A, Rosehart W. Energy storage for mitigating the variability of renewable electricity sources: an updated review. Energy Sustain Dev 2010;14:302–14.
[10] Teleke S, Baran ME, Huang AQ, Bhattacharya S, Anderson L. Control strategies for battery energy storage for wind farm dispatching. IEEE Trans Energy Convers 2009;24:725–32.
[11] Ibrahim H, Ilinca A, Perron J. Energy storage systems – characteristics and comparisons. Renew Sustain Energy Rev 2008;12:1221–50.
[12] Rastler D. Principal investigator, electric energy storage technology options: a white paper primer on applications, costs, and benefits. Palo Alto, CA: Electric Power Research Institute; 2010. p. 1020676 ⟨http://www.epri.com/abstracts/pages/productabstract.aspx?ProductID=000000000001020676⟩ [accessed December 2013].
[13] Dunn B, Kamath H, Tarascon JM. Electrical energy storage for the grid: a battery of choices. Science 2011;334:928–35.
[14] General Electric Company. Products & services: 2.5-120 wind turbine ⟨http://www.ge-energy.com/products_and_services/products/wind_turbines/ges_2.5_120_wind_turbine.jsp⟩ [accessed December 2013].
[15] Howlader AM, Urasaki N, Yona A, Senjyu T, Saber AY. Renew Sustain Energy Rev 2013;26:135–46.
[16] Hadjipaschalis I, Poullikkas A, Efthimiou V. Overview of current and future energy storage technologies for electric power applications. Renew Sustain Energy Rev 2009;13:1513–22.
[17] Divya KC, Østergaard J. Battery energy storage technology for power systems – an overview. Electr Power Syst Res 2009;79:511–20.
[18] Díaz-González F, Sumper A, Gomis-Bellmunt O, Villafáfila-Robles R. A review of energy storage technologies for wind power applications. Renew Sustain Energy Rev 2012;16:2154–71.
[19] Tan X, Li Q, Wang H. Advances and trends of energy storage technology in Microgrid. Electr Power Energy Syst 2013;44:179–91.
[20] Larsen HH, Petersen LS, editors. DTU international energy report 2003. Energy storage options for future sustainable energy systems. Denmark: Technical University of Denmark, ISBN: 978-87-550-3968-1.
[21] Evans A, Strezov V, Evans TJ. Assessment of utility energy storage options for increased renewable energy penetration. Renew Sustain Energy Rev 2012;16:4141–7.
[22] Poullikkas A. A comparative overview of large-scale battery systems for electricity storage. Renew Sustain Energy Rev 2013;27:778–88.
[23] Sandia National Laboratories. Department of energy USA global energy storage database ⟨http://www.energystorageexchange.org/projects⟩ [accessed December 2013].
[24] Cárdenas R, Peña R, Alepuz S, Asher G. Overview of control systems for the operation of DFIGs in wind energy applications. IEEE Trans Ind Electron 2013;60:2776–98.
[25] Sawin JL, lead autor. REN21 renewables 2013 global status report. Paris: REN21 Secretariat; 2013, ISBN: 978-3-9815934-0-2.
[26] Hansen AD, Hansen LH. Wind turbine concept market penetration over 10 years (1995–2004). Wind Energy 2007;10:81–97.
[27] Müller S, Deicke M, de Doncker RW. Doubly fed induction generator systems for wind turbines. IEEE Ind Appl Mag 2002;8:26–33.
[28] Tazil M, Kumar V, Bansal RC, Kong S, Dong ZY, Freitas W. Three-phase doubly fed induction generators: an overview. IET Electr Power Appl 2010;4:75–89.
[29] Engelhardt S, Erlich I, Feltes C, Kretschmann J, Shewarega F. Reactive power capability of wind turbines based on doubly fed induction generators. IEEE Trans Energy Convers 2011;26:364–72.
[30] Meegahapola L, Littler T, Perera S. Capability curve based enhanced reactive power control strategy for stability enhancement and network voltage management. Electr. Power Energy Syst 2013;52:96–106.
[31] Lund T, Sørensen P, Eek J. Reactive power capability of a wind turbine with doubly fed induction generator. Wind Energy 2007;10:379–94.
[32] Tsili M, Papathanassiou S. A review of grid code technical requirements for wind farms. IET Renew Power Gener 2009;3:308–32.
[33] Mohseni M, Islam SM. Review of international grid codes for wind power integration: diversity, technology and a case for a global standard. Renew Sustain Energy Rev 2012;16:3876–90.
[34] Jiang Z, Yu X. Modeling and control of an integrated wind power generation and energy storage system. In: IEEE power & energy society general meeting; 2009. p. 1–8.
[35] Ganti VC, Singh B, Aggarwal SK, Kandpal TC. DFIG-based wind power conversion with grid power leveling for reduced gusts. IEEE Trans Sustain Energy 2012;3:12–20.
[36] Yazdani A. Islanded operation of a doubly-fed induction generator (DFIG) wind-power system with integrated energy storage. In: IEEE Canada electrical power conference; 2007. p. 1–7.
[37] Qu L, Qiao W. Constant power control of DFIG wind turbines with supercapacitor energy storage. IEEE Trans Ind Appl 2011;47:359–67.
[38] Mendis N, Muttaqi KM, Sayeef S, Perera S. Control coordination of a wind turbine generator and a battery storage unit in a remote area power supply system. In: IEEE power & energy society general meeting; 2010. p. 1–7.
[39] Yang TC. Initial study of using rechargeable batteries in wind power generation with variable speed induction generators. IET Renew Power Gener 2008;2:89–101.
[40] Jin C, Wang P. Enhancement of low voltage ride-through capability for wind turbine driven DFIG with active crowbar and battery energy storage system, In: IEEE power & energy society general meeting; 2010. p. 1–8.
[41] Rahim AHMA, Nowicki EP. Supercapacitor energy storage system for fault ride-through of a DFIG wind generation system. Energy Convers Manage 2012;59:96–102.
[42] Morel J, Hiyama T. Energy capacitor system for DFIG-based wind farm transient behavior enhancement. In: IEEE transmission & distribution conference & exposition: Asia and Pacific; 2009. p. 1–4.
[43] Abbey C, Joos G. Supercapacitor energy storage for wind energy applications. IEEE Trans Ind Appl 2007;43:769–76.
[44] Nguyen TH, Lee DC. Improved LVRT capability and power smoothening of DFIG wind turbine systems. J Power Electron 2011;11:568–75.
[45] Fernandez LM, Garcia P, Garcia CA, Jurado F. Comparative study on the performance of control systems for doubly fed induction generator (DFIG) wind turbines operating with power regulation. Energy 2008;33:1438–52.
[46] Chakraborty A. Advancements in power electronics and drives in interface with growing renewable energy resources. Renew Sustain Energy Rev 2011;15:1816–27.
[47] General Electric Company. 1.5 MW series wind turbine ⟨http://www.ge-energy.com/products_and_services/products/wind_turbines/ge_1.5_77_wind_turbine.jsp⟩ [accessed November 2011].
[48] SimPowerSystems™. Reference. Natick, MA: Hydro-Québec/the MathWorks, Inc.; 2010.
[49] Heier S. Grid integration of wind energy conversion systems. Chicester: John Wiley & Sons; 1998.
[50] Krause P, Wasynczuk O, Sudhoff SD. Analysis of electric machinery. IEEE Press; 2002.
[51] Sarrias R, Fernandez LM, Garcia CA, Jurado F. Supervisory control system for DFIG wind turbine with energy storage system based on battery. In: International conference on power engineering, energy and electrical drives; 2011. p. 1–6.
[52] Discover Energy Corp. Datasheet Discover® D series VRLA industrial batteries, part no. D21000 ⟨http://www.discover-energy.com/files/datasheets/D21000.pdf⟩ [accessed November 2011].
[53] Garcia P, Fernandez LM, Garcia CA, Jurado F. Energy management system of fuel cell–battery hybrid tramway. IEEE Trans Ind Electron 2010;57:4013–23.
[54] Fernandez LM, Garcia P, Garcia CA, Torreglosa JP, Jurado F. Comparison of control schemes for a fuel cell hybrid tramway integrating two dc/dc converters. Int J Hydrog Energy 2010;35:5731–44.
[55] Ports of the State (Spanish Public Harbor Operator), Spanish Government. Spanish Ministry of Public Works ⟨http://www.puertos.es/oceanografia_y_meteorologia/redes_de_medida/index.html⟩ [accessed December 2013].